RESEARCH PAPER

Additively Manufactured Porous Titanium Scaffolds for Orthopedic Implants: Design, Mechanical Behavior, and Osseointegration

Shekhar Tanaji Shinde[1], Prof. Prashant D. Yadav[2]*, Prof. Akshay A. Harale[3], Dr. Unmesh S. Pawar[4], Prof. Roheshkumar Sadashiv Lavate[5]

[1,2,3,4,5]Mechanical Engineering Department, Bharati Vidyapeeth Deemed to be University College of Engineering, Pune, India

[1]Email: stshinde@bvucoep.edu.in

[2*]Email: pdyadav@bvucoep.edu.in (Corresponding Author)

[3]Email: aaharale@bvucoep.edu.in

[4]Email: uspawar@bvucoep.edu.in

[5]Email: rslavate@bvucoep.edu.in

ORCID IDs:

Shekhar Tanaji Shinde: https://orcid.org/0000-0001-9941-9626

Prof. Prashant D. Yadav: https://orcid.org/0000-0002-9161-6665

Prof. Akshay A. Harale: https://orcid.org/0000-0001-9788-0208

Dr. Unmesh S. Pawar: https://orcid.org/0000-0001-8586-3988

Prof. Roheshkumar Sadashiv Lavate: https://orcid.org/0000-0002-0506-6864

***Corresponding author: Prof. Prashant D. Yadav, Mechanical Engineering Department, Bharati Vidyapeeth Deemed to be University College of Engineering, Pune, India**

Email: pdyadav@bvucoep.edu.in

ABSTRACT

Additive manufacturing (AM) has emerged as a transformative route for fabricating porous titanium scaffolds with patient-specific geometries and bone-mimicking mechanical responses. By controlling unit-cell architecture, porosity, and surface topography, AM-fabricated Ti and Ti-6Al-4V scaffolds can simultaneously address two long-standing challenges of conventional bulk implants: stress shielding caused by stiffness mismatch between the implant and host bone, and limited osseointegration due to bioinert surfaces. This review synthesizes a decade of progress in laser powder-bed fusion (LPBF), electron-beam melting (EBM), and direct energy deposition (DED) of porous Ti structures for orthopedic applications. The mechanical behavior of strut-based and triply periodic minimal surface (TPMS) lattices is analyzed within the Gibson-Ashby framework, and the role of pore size, porosity, and surface roughness in modulating osseointegration is critically examined, with particular attention to the persistent variance in reported "optimal" pore size (≈178 μm to ≈600 μm) across the literature. Surface modification strategies, defect populations, post-processing routes, and clinical case evidence are discussed, followed by an outlook on β-Ti alloys, biodegradable metals, machine-learning-driven design, and regulatory pathways. The review is intended as a consolidated reference for researchers and clinicians working at the intersection of mechanical engineering, materials science, and orthopedic surgery.

Keywords: additive manufacturing; porous titanium; Ti-6Al-4V; lattice structures; TPMS; orthopedic implants.

How to cite this article: Shinde ST, Yadav PD, Harale AA, Pawar US, Lavate RS. Additively Manufactured Porous Titanium Scaffolds for Orthopedic Implants: Design, Mechanical Behavior, and Osseointegration. Int J Drug Deliv Technol. 2026;16(57s): 859-874. DOI: 10.25258/ijddt.16.57s.90

Source of support: Nil.

Conflict of interest: None.

Abstract

Additive manufacturing (AM) has emerged as a transformative route for fabricating porous titanium scaffolds with patient-specific geometries and bone-mimicking mechanical responses. By controlling unit-cell architecture, porosity, and surface topography, AM-fabricated Ti and Ti-6Al-4V scaffolds can simultaneously address two long-standing challenges of conventional bulk implants: stress shielding caused by stiffness mismatch between the implant and host

bone, and limited osseointegration due to bioinert surfaces. This review synthesizes a decade of progress in laser powder-bed fusion (LPBF), electron-beam melting (EBM), and direct energy deposition (DED) of porous Ti structures for orthopedic applications. The mechanical behavior of strut-based and triply periodic minimal surface (TPMS) lattices is analyzed within the Gibson-Ashby framework, and the role of pore size, porosity, and surface roughness in modulating osseointegration is critically examined, with particular attention to the persistent variance in reported "optimal" pore size (≈178 μm to ≈600 μm) across the literature. Surface modification strategies, defect populations, post-processing routes, and clinical case evidence are discussed, followed by an outlook on β-Ti alloys, biodegradable metals, machine-learning-driven design, and regulatory pathways. The review is intended as a consolidated reference for researchers and clinicians working at the intersection of mechanical engineering, materials science, and orthopedic surgery.

Keywords: additive manufacturing; porous titanium; Ti-6Al-4V; lattice structures; TPMS; orthopedic implants;

1. Introduction

Bone defects arising from trauma, degenerative disease, congenital abnormality, or oncological resection remain a major clinical burden worldwide [1,2]. Traditional metallic implants - most commonly fabricated from 316L stainless steel, cobalt-chromium alloys, and bulk titanium alloys - have been used for decades to restore load-bearing function [3]. While these materials offer adequate strength and corrosion resistance, two limitations restrict their long-term clinical performance. First, the elastic modulus of conventional metals (110 GPa for Ti-6Al-4V; 200 GPa for stainless steel) far exceeds that of cortical bone (≈10-20 GPa) and cancellous bone (≈0.1-2 GPa), giving rise to stress shielding and progressive peri-implant bone resorption [4,5]. Second, the smooth, dense surfaces of machined implants are bioinert, providing limited mechanical interlock and slow osseointegration, which together can lead to aseptic loosening over service lifetimes of 10-20 years [6,7].

Additive manufacturing (AM) - also referred to as metal 3D printing - has changed the design space available to orthopedic engineers [8]. By building components layer-by-layer from a powder or wire feedstock, AM enables the fabrication of geometries that are extremely difficult or impossible to produce by casting, forging, or subtractive machining. In particular, AM allows the controlled introduction of internal porosity at length scales relevant to bone tissue (50-1000 μm), with strut diameters and pore architectures that can be designed to match the modulus and strength of bone while simultaneously promoting cell infiltration, vascularization, and bone ingrowth [9,10]. The global orthopedic implant market, valued at over US$55 billion in 2022 [11], increasingly incorporates AM-fabricated patient-specific solutions, with notable clinical adoption in spinal cages, acetabular cups, cranio-maxillofacial reconstruction, and custom limb-salvage implants [12]. Porous Ti and Ti-6Al-4V scaffolds produced by laser powder-bed fusion (LPBF) and electron-beam melting (EBM) have therefore become the focus of intense research over the past decade [13,14]. Recent advances span unit-cell topology optimization, the introduction of triply periodic minimal surface (TPMS) lattices such as gyroid and Schwarz primitive, β-titanium alloy compositions with reduced elastic moduli, and surface modification strategies that combine micro/nano roughness, hydroxyapatite coating, and drug delivery functions [15-18]. However, the literature is fragmented across mechanical-engineering, materials-science, and biomedical journals, and reported "optimal" parameters - particularly pore size and porosity - vary widely between studies [19,20]. This review aims to consolidate that fragmented body of work into a single critical synthesis, with three guiding objectives: (i) to compare AM processes in terms of process windows, achievable resolutions, and resulting microstructures; (ii) to analyze the mechanical behavior of strut-based and TPMS lattices through the Gibson-Ashby framework; and (iii) to critically interpret the variance in reported pore-size optima for osseointegration.

2. Background on Titanium Alloys for Orthopedic Use

Titanium and its alloys are the dominant metallic biomaterials for load-bearing orthopedic implants because of their high specific strength, excellent corrosion resistance in physiological environments, and acceptable biocompatibility [21,22]. Three families are most commonly encountered: commercially pure titanium (CP-Ti), the α+β alloy Ti-6Al-4V, and emerging β-titanium alloys.

2.1 Commercially Pure Titanium (CP-Ti)

CP-Ti grades 1-4 differ primarily in interstitial oxygen content and exhibit ultimate tensile strengths of 240-550 MPa with elastic moduli of 100-110 GPa [23]. CP-Ti is widely used in dental implants and small osteosynthesis devices but is generally too soft for

high-load orthopedic joints. Its excellent biocompatibility and the spontaneous formation of a protective TiO_2 surface layer remain a benchmark against which alloyed materials are compared [24].

2.2 Ti-6Al-4V (Grade 5 and Grade 23 ELI)

Ti-6Al-4V is the workhorse alloy in orthopedic AM, offering ultimate tensile strength of 900-1100 MPa and a fatigue limit of 500-600 MPa in wrought form [25]. The extra-low interstitial (ELI) Grade 23 variant has reduced oxygen and iron content, enhancing fracture toughness for biomedical use. Concerns regarding long-term release of vanadium and aluminum ions - implicated in cytotoxicity and Alzheimer-related neurotoxicity in some in vitro studies - have driven research into alternative compositions, but Ti-6Al-4V continues to dominate AM implant production due to its mature processing windows and regulatory familiarity [26,27].

2.3 β-Titanium Alloys

β-stabilized titanium alloys such as Ti-13Nb-13Zr, Ti-29Nb-13Ta-4.6Zr (TNTZ), and Ti-24Nb-4Zr-8Sn use non-toxic alloying elements (Nb, Zr, Ta, Sn, Mo) and offer elastic moduli as low as 40-60 GPa - substantially closer to cortical bone than Ti-6Al-4V [28,29]. Combined with porous AM architectures, β-alloys can therefore reduce stress shielding through both compositional and structural means. Their chief disadvantage is processing difficulty: Nb and Ta have very high melting points, increasing the risk of partial melting and elemental segregation in LPBF [30].

Table 1: Typical mechanical properties of titanium alloys used in orthopedic AM compared with bone reference values [21,28,29].

Alloy	Typical UTS (MPa)	Elastic Modulus E (GPa)	Primary Orthopedic Use
CP-Ti (Grade 4)	550	105	Dental, small osteosynthesis
Ti-6Al-4V (Grade 5)	900-1100	110	Joint stems, plates, scaffolds
Ti-6Al-4V ELI (Grade 23)	860-965	114	Long-term biomedical implants
Ti-13Nb-13Zr	850-1030	79-84	Stems, low-modulus scaffolds
Ti-29Nb-13Ta-4.6Zr (TNTZ)	590-700	55-65	Research β-alloy, bone-matched
Ti-24Nb-4Zr-8Sn	700-800	≈42	Low-modulus orthopedic research
Cortical bone	100-230	10-20	-
Cancellous bone	1-10	0.1-2	-

3. Additive Manufacturing Processes for Porous Titanium

ASTM F2792 classifies metal AM processes into seven categories, of which three are relevant to porous Ti scaffolds: powder bed fusion (PBF), directed energy deposition (DED), and binder jetting (BJ). PBF processes - laser powder-bed fusion (LPBF, also termed selective laser melting, SLM) and electron-beam melting (EBM) - dominate orthopedic scaffold fabrication because of their ability to resolve fine struts (<200 µm) and complex internal channels [31,32].

3.1 Laser Powder-Bed Fusion (LPBF / SLM)

LPBF uses a high-power fiber laser (typically 200-500 W) to selectively melt a thin layer (20-60 µm) of pre-spread Ti powder under an inert argon atmosphere. The build is performed at near-room ambient temperature with a heated baseplate (typically 100-200 °C). LPBF achieves the finest feature resolution among metal AM methods (≈100-150 µm minimum strut diameter) and produces a martensitic α′ microstructure with high yield strength but limited ductility, requiring post-build heat treatment to improve fatigue performance [33]. Critical parameters are laser power (P), scan speed (v), hatch spacing (h), and layer thickness (t), commonly combined into the volumetric energy density $Ev = P/(v \cdot h \cdot t)$ (J/mm³). For Ti-6Al-4V, Ev values of 50-80 J/mm³ typically yield >99.5% relative density [34]. as illustrated in Figure 1

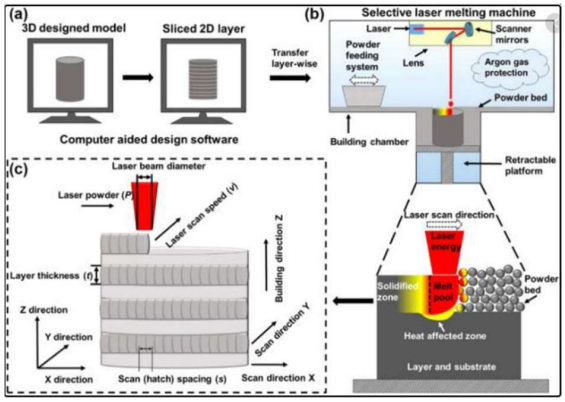

Figure 1: Schematic representation of the selective laser melting process: (a) CAD model and slicing, (b) powder-bed system, and (c) melt-pool/layer formation. [13]

3.2 Electron-Beam Melting (EBM)

EBM uses a focused electron beam in a high vacuum (≈10^{-5} mbar) to melt powder layers under elevated build temperatures (≈700 °C for Ti-6Al-4V). The high vacuum suppresses oxygen pickup and the elevated temperature anneals the structure during the build, producing α+β lamellar microstructures with higher ductility and lower residual stress than as-built LPBF parts [35,36]. EBM uses thicker layers (50-100 µm) and coarser powder (45-105 µm), yielding faster build rates but coarser surface finishes and a minimum strut diameter of approximately 200-300 µm [37].

3.3 Directed Energy Deposition (DED)

DED includes laser DED (LP-DED) using powder feed and wire arc additive manufacturing (WAAM) using wire feed. DED achieves much higher deposition rates (kg/h) than PBF but with coarser resolution (1-5 mm minimum feature size), making it unsuitable for fine lattice scaffolds. DED is, however, increasingly used for large structural orthopedic components such as custom long-bone replacements where coarser internal porosity is acceptable, and for repair of existing implants [38].

3.4 Process Comparison and Selection

Process selection is governed by the trade-off between resolution, build size, microstructure, and surface finish. Table 2 summarizes the principal differences.

Table 2: Comparison of the principal AM processes used to fabricate porous titanium orthopedic scaffolds [31-37].

Attribute	LPBF (SLM)	EBM	Laser DED
Energy source	Fiber laser (200-500 W)	Electron beam (3-6 kW)	Laser (1-6 kW)
Atmosphere	Argon (inert)	Vacuum (~10^{-5} mbar)	Argon shielding
Build temperature	100-200 °C	≈700 °C	Ambient
Powder size (µm)	15-45	45-105	45-150
Layer thickness (µm)	20-60	50-100	200-1000
Min. strut diameter (µm)	100-150	200-300	1000+
Surface roughness Ra (µm)	8-15	20-40	20-50
As-built microstructure	Martensitic α′	α+β lamellar	α+β columnar
Residual stress	High	Low	Moderate
Typical scaffold use	Fine lattices, TPMS	Acetabular cups, EBM lattices	Large segmental bone

4. Scaffold Design: Strut-Based vs. TPMS Architectures

The mechanical and biological response of a porous scaffold is governed primarily by its internal architecture. Two broad classes dominate the literature: (i) strut-based lattices, derived from periodic tessellation of polyhedral unit cells, and (ii) triply periodic minimal surface (TPMS) lattices, derived from implicit surface equations [39,40]. The choice between them shapes both load-bearing behavior (Section 5) and the local fluid mechanics that govern cell migration and nutrient transport (Section 6).

4.1 Strut-Based Lattices

Strut-based unit cells are constructed from straight cylindrical or prismatic struts joined at nodesas shown in figure 2(a). Common topologies include the simple cubic, body-centered cubic (BCC), face-centered cubic (FCC), octet-truss, diamond, and rhombic dodecahedron [41]. Their mechanical behavior is classified as either bending-dominated or stretch-dominated, following Maxwell's stability criterion $M = b - 3n + 6$, where b is the number of struts and n the number of nodes. $M < 0$ yields bending-dominated behavior (e.g., BCC, diamond) with relatively compliant response and high energy absorption, while $M \geq 0$ yields stretch-dominated behavior (e.g., octet-truss) with higher stiffness and strength at a given relative density [42,43].

Strut-based lattices are computationally simple to design and have been the workhorse of early scaffold studies. Their principal disadvantages are (i) sharp stress concentrations at strut-node junctions, which initiate fatigue cracks under cyclic load, and (ii) relatively poor permeability anisotropy, which can produce direction-dependent fluid flow and cell-seeding heterogeneity [44].

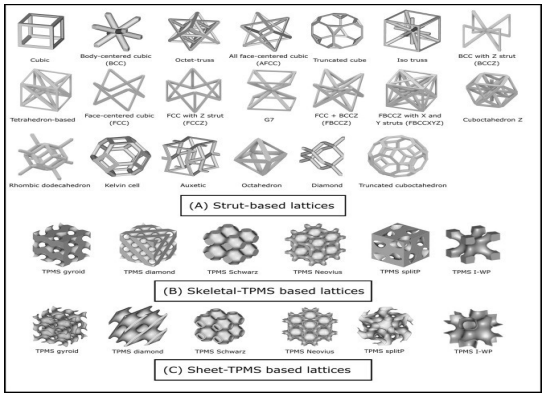

Figure 2. Various architectures of lattice structures (A) Strut-based lattice cells are shown in the first three rows. (B) Skeletal- and (C) sheet-based triply periodic minimal surfaces (TPMS) [100]

4.2 Triply Periodic Minimal Surface (TPMS) Lattices

TPMS structures as shown in figure 2(c) are mathematically defined by implicit equations describing surfaces of zero mean curvature that repeat in three orthogonal directions. The two most studied for orthopedic scaffolds are the Schoen gyroid and the Schwarz primitive (Schwarz P), with approximate level-set forms:

$$Gyroid: \quad \sin(x)\cdot\cos(y) + \sin(y)\cdot\cos(z) + \sin(z)\cdot\cos(x) = c$$

$$Schwarz\ P: \quad \cos(x) + \cos(y) + \cos(z) = c$$

where c is a level-set constant that controls the relative volume fraction (and thus porosity), and (x, y, z) are scaled by the unit-cell length. By thickening the surface (sheet-TPMS) or filling one of the two interpenetrating sub-volumes (skeletal-TPMS), solid scaffolds with two fully connected, interpenetrating pore networks are obtained [45].

TPMS lattices offer three documented advantages over strut-based topologies. First, the smooth, curvature-continuous surfaces eliminate sharp stress concentrators, raising the fatigue limit by 20-60% at equivalent relative density [46]. Second, the bicontinuous pore network produces near-isotropic permeability and more uniform fluid shear stress, both favorable for cell migration and vascularization [47]. Third, the topology mimics the natural surface curvature of trabecular bone, which has been linked in vitro to enhanced osteoblast differentiation [48].

4.3 Direct Comparison: Gyroid vs. Schwarz P vs. Octet-Truss

At equivalent relative density (≈0.30), the gyroid sheet-TPMS exhibits a slightly lower elastic modulus than the Schwarz P sheet-TPMS but markedly higher fatigue endurance and more isotropic stiffness. The Schwarz P, with its straight orthogonal channels, presents the largest unobstructed pore openings, favoring cell seeding through flow perfusion bioreactors but creating mild stiffness anisotropy along the principal axes. The octet-truss, a stretch-dominated strut lattice, achieves the highest specific stiffness but suffers the lowest fatigue ratio ($\sigma e/\sigma y \approx 0.20$) due to severe node stress concentrations [49]. Table 3 summarizes the main qualitative trends.

Table 3: Qualitative comparison of representative strut-based and TPMS lattice topologies for porous Ti orthopedic scaffolds [39-49].

Attribute	Octet-truss (strut)	Diamond (strut)	Gyroid (TPMS)	Schwarz P (TPMS)
Maxwell number M	≥ 0 (stretch)	< 0 (bending)	N/A (curvature)	N/A (curvature)
Relative stiffness	Highest	Moderate	High	High (anisotropic)
Stress concentration	High at nodes	High at nodes	Very low	Low
Fatigue ratio σ_e/σ_y	≈ 0.20	≈ 0.25	≈ 0.40-0.50	≈ 0.35-0.45
Permeability isotropy	Poor	Moderate	Excellent	Anisotropic
Manufacturability (LPBF)	Easy	Easy	Moderate	Moderate
Suitability for cell ingrowth	Moderate	Good	Excellent	Excellent

5. Mechanical Behavior of Porous Titanium Scaffolds

The defining mechanical objective of a porous orthopedic scaffold is to match the elastic modulus of the host bone to mitigate stress shielding while retaining sufficient yield strength and fatigue endurance to survive cyclic physiological loading. The Gibson-Ashby cellular solids framework provides the standard analytical basis for relating scaffold mechanical properties to relative density [50] as illustrated in figure 3.

5.1 The Gibson-Ashby Framework

Gibson and Ashby derived scaling laws relating the macroscopic (effective) properties of a cellular solid to its base-material properties through the relative density ρ*/ρs, where ρ* is the apparent density of the porous structure and ρs is the density of the fully dense parent material. For the elastic modulus:

$$E^*/E_s = C_1 \cdot (\rho^*/\rho_s)^n$$

and for the plateau (yield/collapse) stress:

$$\sigma^*/\sigma_{ys} = C_2 \cdot (\rho^*/\rho_s)^m$$

where E* and σ* are the effective scaffold modulus and yield stress, E_s and σ_{ys} are the corresponding base-material properties, and C_1, C_2, n, and m are dimensionless scaling factors that depend on cell geometry and deformation mode. For an idealized open-cell foam dominated by strut bending, Gibson and Ashby's theoretical analysis gives $C_1 \approx 1$, $n \approx 2$, $C_2 \approx 0.3$, and $m \approx 1.5$. For closed-cell or stretch-dominated lattices, n approaches 1 and the structure scales much more efficiently with density [50,51].

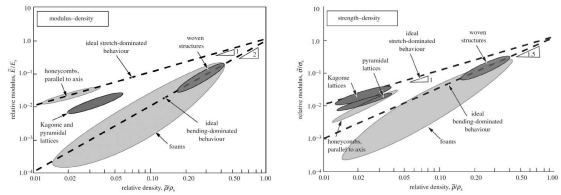

Figure 3: (a) Gibson-Ashby model: relative modulus against relative density, (b) Gibson-Ashby model: relative strength against relative density [43]

Experimentally determined scaling factors for AM Ti-6Al-4V scaffolds are summarized in Table 4. Bending-dominated topologies such as BCC and diamond consistently exhibit n ≈ 2.0-2.3, in excellent agreement with theory. Stretch-dominated lattices such as the octet-truss and rhombic dodecahedron show n ≈ 1.0-1.5, indicating more efficient stiffness scaling. TPMS lattices fall between these limits (n ≈ 1.4-1.8), reflecting their mixed deformation mode in which membrane stretching, bending, and curvature effects all contribute [52,53].

Table 4: Experimentally measured Gibson-Ashby scaling factors for AM Ti-6Al-4V lattices in compression. Values are typical literature ranges for relative densities of 0.15-0.40.

Topology	Deformation mode	C_1 (modulus)	n (modulus exponent)	Reference
BCC strut	Bending-dominated	0.6-0.9	2.0-2.3	[51,52]
Diamond strut	Bending-dominated	0.7-1.0	2.0-2.2	[52]

Topology	Deformation mode	C_1 (modulus)	n (modulus exponent)	Reference
Octet-truss	Stretch-dominated	0.3-0.5	1.0-1.4	[53]
Rhombic dodecahedron	Mixed	0.4-0.7	1.5-1.8	[52]
Gyroid (sheet)	Curvature/membrane	0.5-0.8	1.4-1.7	[46,47]
Schwarz P (sheet)	Curvature/membrane	0.5-0.8	1.5-1.8	[47]

5.2 Modulus Matching to Bone

Cortical bone has an elastic modulus of 10-20 GPa and cancellous bone of 0.1-2 GPa [4]. To eliminate stress shielding in load-bearing applications, the scaffold modulus should fall within or just below this range. Using Ti-6Al-4V ($E_s \approx 110$ GPa) as the base material and a bending-dominated lattice ($C_1 \approx 0.7$, $n \approx 2.1$), the relative density required to achieve $E^* = 15$ GPa is approximately 0.43, corresponding to a porosity of 57%. Stretch-dominated lattices reach the same target stiffness at lower relative density (≈0.32, porosity 68%), giving more pore volume for tissue ingrowth at the cost of a smaller fatigue safety margin [54].

5.3 Fatigue and Cyclic Loading

Fatigue performance is the most demanding mechanical requirement for permanent orthopedic implants, which must survive $\geq 10^7$ cycles in vivo. AM Ti-6Al-4V lattices typically show fatigue ratios ($\sigma e/\sigma y$) of 0.10-0.50 depending on topology and surface state. As-built rough surfaces can reduce the fatigue limit by 30-50% relative to machined surfaces because of micro-notch effects associated with partially adhered powder [55]. Hot isostatic pressing (HIP) and chemical/electrochemical polishing routinely recover much of this loss [56]. TPMS lattices have repeatedly been shown to outperform strut-based lattices of equal relative density in fatigue, primarily through elimination of node stress concentrators [46,49].

6. Biological Performance and Osseointegration

Mechanical compatibility alone is insufficient: a successful scaffold must also support cell attachment, proliferation, vascular ingrowth, and ultimately new bone formation. The biological response is governed by a combination of pore size, porosity, surface roughness, surface chemistry, and local fluid mechanics [57,58]. Among these, pore size has received the most attention - and produced the largest spread of reported optima.

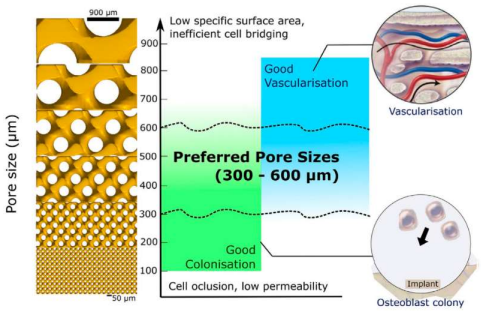

Figure 4 : A tradeoff between bone colonization and vascularization in terms of pore size. [99]

6.1 General Trends in Pore Size and Porosity

Across two decades of in vitro and in vivo studies, three broad pore-size regimes are consistently identified [9,57]. Pores below ~100 µm are too small for vascular ingrowth and tend to limit bone formation to surface apposition. Pores between ~100 and 1000 µm support both vascularization and mineralized bone ingrowth, with most reports placing the optimum somewhere in the 300-600 µm range illustrated in Figure 4 and Figure 5. Pores above ~1000 µm reduce the surface area available for cell attachment and reduce mechanical performance disproportionately. Porosity (volume fraction of voids) is typically reported as optimal in the range of 60-80%, balancing biological permeability against mechanical integrity [59,60].

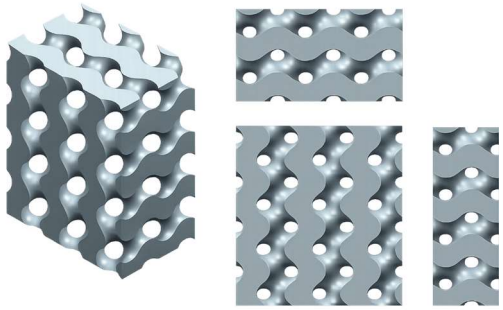

Figure 5: Ti-6Al-4V scaffolds in osseointegration studies. The shaded vertical band indicates the consensus 300-600 µm window

6.2 Critical Analysis: The 178 µm vs. 600 µm Question

Despite the broad consensus on the 300-600 µm range, individual studies have repeatedly identified "optimal" pore sizes spanning a much wider window. Kapat et al. compared LPBF Ti-6Al-4V scaffolds with nominal pore sizes of 92, 178, and 297 µm and reported the highest bone volume fraction (~52% greater than the other groups) at 178 µm after 12 weeks of in vivo implantation [61]. Ran et al., examining LPBF Ti-6Al-4V cubes with nominal pore sizes of 500, 700, and 900 µm (actual sizes 400, 600, 800 µm), found the best biological performance at 600 µm [62]. Luan et al. compared 334, 383, and 401 µm and identified 383 µm as optimal [63]. Taken at face value, these reports appear contradictory.

Three methodological factors largely explain the variance. First, design pore size and as-built pore size differ substantially in LPBF - partially adhered powder, melt-pool overshoot, and staircase effects can shrink nominal pores by 20-40%, so a "178 µm" design may be functionally similar to a "297 µm" design from a different group. Many of the studies identifying small "optimal" pores measured nominal CAD values rather than as-built micro-CT values [64]. Second, the compared range matters: a study comparing 92, 178, and 297 µm cannot detect that 600 µm might be better still - the optimum reported is the best of the three, not the global optimum. Third, the biological readout differs: bone volume fraction at 12 weeks, push-out strength at 8 weeks, and ALP activity at 14 days do not weight pore size identically [65].

When studies are restricted to those that (i) report as-built pore sizes via micro-CT, (ii) compare a sufficiently wide range, and (iii) use long in vivo follow-up, the operative window narrows to approximately 300-600 µm, with values closer to 400-500 µm appearing most consistent for cortical-bone applications. The often-cited 178 µm result is best interpreted not as a contradiction but as evidence that, at smaller scales, vascularization remains adequate provided permeability is preserved by interconnected channels - a condition more easily met by TPMS than by strut lattices [66]. Pore-size selection should therefore be made jointly with topology and porosity, not as a stand-alone parameter.

6.3 Surface Roughness and Cell Behavior

AM Ti scaffolds inherit a surface roughness Ra of 8-15 µm (LPBF) or 20-40 µm (EBM) from partially adhered powder and the layered build process [37]. This roughness scale falls within the same order of magnitude as osteoblast cells (10-30 µm) and has been repeatedly shown to enhance cell attachment, focal-adhesion formation, and osteogenic differentiation relative to polished surfaces [67]. However, very rough surfaces also harbor un-melted powder particles that can detach in vivo and elicit inflammatory responses, so a deliberate post-processing strategy that retains micro-roughness while removing loose particles is generally preferred [68].

6.4 Permeability and Fluid Flow

Permeability k (m^2) governs the rate at which interstitial fluid, nutrients, and signaling molecules can transport through the scaffold. Trabecular bone permeability is typically 10^{-11} to 10^{-9} m^2. Scaffolds with permeability below this range may starve interior regions of nutrients, leading to a "dead core" phenomenon, while excessive permeability reduces wall shear stress on attached cells below mechanotransductive thresholds. TPMS lattices, with their bicontinuous pore networks, achieve more uniform permeability than strut lattices and are increasingly preferred for thick scaffolds (>10 mm) [47,69].

7. Surface Modification and Functionalization

Even with optimized macro- and meso-scale architecture, the bioinert nature of native TiO_2 limits the rate of osseointegration. Surface modification at the micro- and nano-scale, and the addition of bioactive coatings, are therefore standard supplements to scaffold design [16,70].

7.1 Chemical and Electrochemical Treatments

Acid etching (HF/HNO_3 or HCl/H_2SO_4), alkaline treatment (NaOH followed by heat), and anodization (yielding TiO_2 nanotube arrays) are widely used to generate hierarchical surface topographies that enhance protein adsorption and osteoblast adhesion [71,72]. Anodization in particular allows precise control of nanotube diameter (typically 30-100 nm), with diameters near 70 nm reported to favor osteogenic differentiation of mesenchymal stem cells.

7.2 Bioceramic Coatings

Hydroxyapatite (HA) and other calcium phosphate-based bioceramic coatings are widely used to improve the biological performance of titanium and Ti-6Al-4V

orthopedic implants. Since HA is chemically similar to the mineral phase of natural bone, HA-coated Ti surfaces can enhance protein adsorption, osteoblast attachment, early bone bonding, and interfacial osseointegration. In additively manufactured porous Ti scaffolds, such coatings are particularly useful because they can functionalize the internal pore surfaces while retaining the load-bearing role of the metallic framework.

Conventional HA coatings may be deposited by plasma spraying, electrochemical deposition, sol-gel processing, hydrothermal treatment, or biomimetic immersion. However, coating stability remains an important concern, especially under cyclic orthopedic loading. Thick plasma-sprayed coatings may suffer from cracking or delamination, whereas thinner electrochemical or hydrothermal coatings generally provide better adhesion to complex porous surfaces.

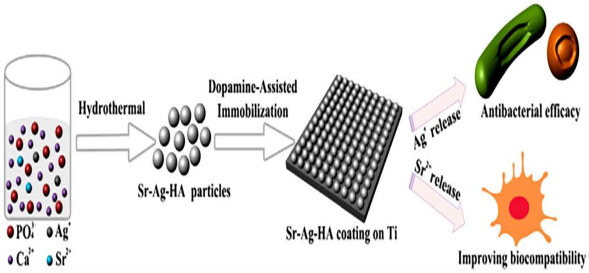

Figure 6. Schematic illustration of Sr/Ag-doped hydroxyapatite coating on Ti implants, showing hydrothermal particle preparation, dopamine-assisted immobilization, ion release, antibacterial activity, and improved biocompatibility [101]**.**

Recent coating strategies therefore focus not only on osteoconductivity but also on multifunctional biological activity. For example, Sr/Ag-doped HA coatings combine the bone-supporting effect of HA with the biological roles of strontium and silver ions. Strontium incorporation can support osteogenic activity and improve implant–bone interaction, while silver ion release provides antibacterial protection at the implant surface. As shown in **Figure 6**, Sr/Ag-doped HA particles can be prepared through a hydrothermal route and immobilized on Ti surfaces, producing a functional coating capable of releasing Ag^{+} and Sr^{2+} ions. This type of surface modification is especially relevant for porous orthopedic implants, where infection control and rapid osseointegration are both critical for long-term clinical success.

7.3 Bioactive Loading and Drug Delivery

The internal porosity of AM scaffolds offers a built-in reservoir for local delivery of antibiotics (vancomycin, gentamicin), anti-resorptive agents (bisphosphonates), or osteogenic factors (BMP-2, dexamethasone). Loading is typically achieved by impregnation in a polymeric or hydrogel carrier infused into the pore network, allowing controlled release over days to weeks [75,76]. This dual mechanical-pharmacological function is increasingly viewed as a defining advantage of porous AM scaffolds over conventional implants.

8. Defects, Limitations, and Quality Control

AM-fabricated porous Ti is subject to a characteristic set of defects that arise from the layer-by-layer melting process and that critically influence both mechanical performance and regulatory acceptance [77].

8.1 Porosity Defects

Three porosity types are commonly distinguished. Lack-of-fusion porosity, caused by insufficient energy input (low Ev), produces irregular voids elongated parallel to the build plane and is the most damaging to fatigue life. Keyhole porosity, caused by excessive energy input, produces near-spherical pores from vapor entrapment within deep melt pools. Gas porosity, originating from dissolved gas in the powder, is typically small (<50 µm) and spherical. All three reduce effective load-bearing cross-section and act as fatigue-crack initiators [78,79].

8.2 Residual Stress and Distortion

The high cooling rates of LPBF (10^4-10^6 K/s) generate steep thermal gradients and compressive surface / tensile sub-surface residual stresses on the order of several hundred MPa. In thin lattice struts these stresses can cause distortion, delamination from the baseplate, or even mid-build cracking. EBM, with its elevated build temperature, produces substantially lower residual stress [35].

8.3 Surface Quality and Partially Adhered Powder

The as-built surfaces of LPBF and EBM lattices retain partially fused powder particles that increase Ra, reduce fatigue performance, and represent a source of debris in vivo. Effective post-processing therefore typically combines hot isostatic pressing (HIP) for internal porosity, heat treatment for microstructure, and chemical etching, abrasive flow machining, or electropolishing for surface finishing [80,81].illustrated as figure 7

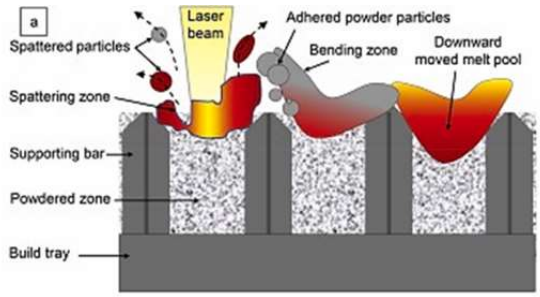

Figure 7: Schematic diagram of surface defects during layer by layer scanning [102],

8.4 Quality Control and In-situ Monitoring

Conventional non-destructive evaluation by micro-CT remains the reference standard for porous AM parts but is slow and expensive. In-situ process monitoring - using high-speed thermal cameras, photodiodes, and acoustic sensors during the build - combined with machine-learning-based defect classification has emerged as a practical route toward real-time quality assurance [82,83].

Table 5: Typical defects in AM porous Ti scaffolds, their causes, and standard mitigation strategies [77-82].

Defect type	Typical cause	Morphology	Mitigation
Lack-of-fusion	Insufficient energy density	Irregular, layer-aligned	Increase P or reduce v; optimize hatch
Keyhole porosity	Excessive energy density	Spherical, sub-surface	Reduce P; increase v
Gas porosity	Dissolved gas in powder	Small, spherical	Use atomized powder; HIP
Residual stress	Steep thermal gradients	Distortion, cracking	Stress-relief heat treatment; EBM
Adhered powder	Powder near melt pool partially fuses	Surface particles	Chemical etching; electropolishing
Strut undersize	Beam offset, melt-pool size	Reduced strut diameter	Calibrate beam compensation

9. Clinical Applications and Case Studies

AM porous Ti scaffolds have transitioned from research prototypes to clinically deployed devices over the past decade. Several application domains illustrate the maturity of the technology [12,84].

9.1 Spinal Interbody Cages

Porous EBM Ti-6Al-4V interbody fusion cages are now among the most widely used AM orthopedic devices. Their porous outer surfaces promote bony fusion across the disc space, while internal trabecular-like architecture reduces stiffness mismatch with adjacent vertebrae. Multi-year follow-up studies report fusion rates competitive with or superior to traditional PEEK and bulk-Ti cages [85].

9.2 Acetabular Cups and Hip Components

EBM-built porous acetabular cups with lattice or stochastic-foam outer surfaces have been clinically implanted for over a decade. The porous surface obviates the need for separate plasma-sprayed coatings and provides immediate mechanical fixation [86].as illustrated in figure 8.

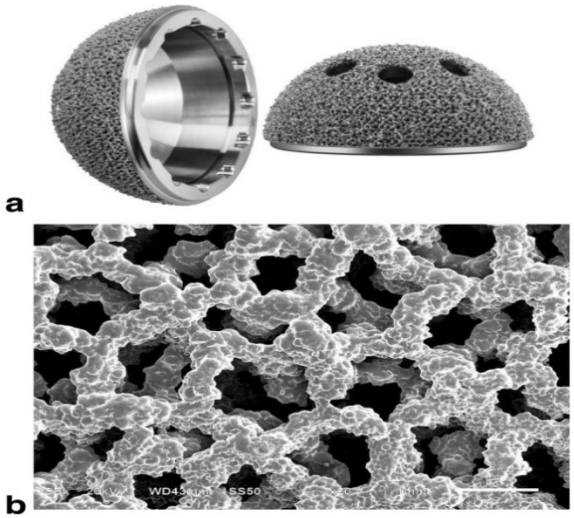

Figure 8: (a)The picture shows the 3D ACT EBM-produced trabecular titanium acetabular cup (b) and the SEM image of its interconnected trabecular titanium cellular solid structure showed the porous

architecture was designed based on a dodecahedron unit cell [103]

9.3 Custom Limb-Salvage and Oncological Implants

Patient-specific implants for tumor resection - including custom hemipelvic prostheses, scapulae, and segmental long-bone replacements - are an area where AM is uniquely enabling. CT-derived geometry is used to design an implant that exactly fills the resection defect, with a porous interface region for bony integration [87].

9.4 Cranio-Maxillofacial Reconstruction

Mandibular, orbital floor, and cranial vault reconstructions using patient-specific porous Ti implants now form a standard part of the maxillofacial surgeon's toolkit, with reported soft-tissue and functional outcomes that exceed those of pre-AM techniques [88].

9.5 Dental Implants

Although the dental implant market remains dominated by conventional machined screws, AM is making inroads through patient-specific root-form implants and subperiosteal frameworks for severely atrophic jaws [89].

10. Challenges and Future Directions

10.1 Regulatory and Standardization Challenges

Despite clinical success, AM porous Ti scaffolds face persistent regulatory scrutiny. The FDA's 2017 guidance "Technical Considerations for Additive Manufactured Medical Devices" and parallel EU MDR pathways require comprehensive control of powder lot variability, build-to-build reproducibility, and post-processing. ASTM/ISO standards (ASTM F3001, ISO/ASTM 52900) are evolving but do not yet cover all relevant scaffold-specific parameters such as as-built pore size tolerance and lattice fatigue testing protocols [90,91].

10.2 Beyond Ti-6Al-4V: β-Alloys and Biodegradable Metals

β-titanium alloys (Ti-Nb-Zr, Ti-Nb-Ta) remain a strong avenue for further reduction of stress shielding through compositional tuning [28,29]. In parallel, biodegradable metals - magnesium, zinc, and iron alloys - are being explored as temporary scaffolds that resorb at a rate matched to bone healing, eliminating the need for revision surgery in pediatric and trauma applications [92,93]. AM of biodegradable metals is technically more challenging due to high vapor pressure (Mg) or sluggish dissolution kinetics (Fe), but rapid progress has been reported in the past three years.

10.3 Machine-Learning-Driven Design

Topology optimization and machine learning are converging to accelerate the design of patient-specific scaffolds. Generative design algorithms can produce graded, anatomy-matched lattices in minutes that would take days by hand. Surrogate models trained on finite-element and bone-remodeling simulations can predict in vivo performance with reasonable accuracy, opening the door to closed-loop patient-specific design-manufacture-implant pipelines [94,95].

10.4 Multi-Material and Functionally Graded Structures

Functionally graded scaffolds - with smoothly varying porosity, pore size, or material composition through the scaffold thickness - better mimic the natural cortical-to-cancellous transition in bone. Multi-material AM, including hybrid metal-polymer and metal-ceramic structures, is enabling locally tailored mechanical and biological properties [96,97].

10.5 In-situ Monitoring and Digital Twins

The combination of in-situ thermal/optical monitoring and physics-informed digital twins of the build process is moving AM toward genuinely qualified, traceable production for medical devices. This is expected to be the dominant trajectory for the next 5-10 years [98].

11. Conclusion

Additively manufactured porous titanium scaffolds have moved decisively from laboratory curiosity to clinical reality. The combination of LPBF and EBM with carefully designed lattice architectures - and increasingly with TPMS topologies - enables implants whose stiffness, strength, and pore network can be tuned simultaneously to match host bone and to support osseointegration. The Gibson-Ashby framework provides a robust analytical bridge between scaffold design and mechanical performance, while two decades of biological studies have converged on a 300-600 μm pore-size window and 60-80% porosity as a workable starting point, with the remaining variance largely attributable to differences in measurement methodology and topology rather than fundamental biological disagreement. Key open challenges remain. Fatigue qualification of complex lattices, regulatory standardization of pore-level dimensional tolerance, and routine in-situ defect

detection are all active research fronts. Looking forward, the integration of β-titanium alloys, biodegradable metals, machine-learning-driven generative design, and multi-material functionally graded architectures promises a next generation of scaffolds that are simultaneously patient-specific, mechanically bone-matched, biologically active, and pharmacologically functional. For mechanical and biomedical engineers entering this field, the design space is rich, the clinical need is clear, and the tools - from modern LPBF systems to TPMS-aware CAD - are unprecedented in their accessibility.

Author Contributions

Shekhar Tanaji Shinde contributed to conceptualization, supervision, methodology, technical guidance, manuscript editing, and final approval. Prof. Prashant D. Yadav contributed to literature review, data interpretation, manuscript drafting, figures, tables, references, and revision. Prof. Akshay A. Harale, Dr. Unmesh S. Pawar, and Prof. Roheshkumar S. Lavate provided technical review and final approval.

Funding

The authors received no specific funding from any public, commercial, or not-for-profit funding agency for the preparation of this review article.

Conflict of Interest

The authors declare that they have no known competing financial interests or personal relationships that could have influenced the work reported in this manuscript.

Ethical Approval

Ethical approval was not required for this study because the manuscript is a review article based on previously published literature and does not involve human participants, animal experiments, or patient-specific clinical data.

Data Availability Statement

No new experimental data were generated or analyzed in this review article. All information discussed in the manuscript was obtained from previously published literature and is available from the cited sources.

References

[1] Roseti L, Parisi V, Petretta M, Cavallo C, Desando G, Bartolotti I, et al. Scaffolds for bone tissue engineering: state of the art and new perspectives. Mater Sci Eng C. 2017;78:1246-1262.

[2] Florencio-Silva R, Sasso GRS, Sasso-Cerri E, Simoes MJ, Cerri PS. Biology of bone tissue: structure, function, and factors that influence bone cells. Biomed Res Int. 2015;2015:421746.

[3] Geetha M, Singh AK, Asokamani R, Gogia AK. Ti based biomaterials, the ultimate choice for orthopaedic implants: a review. Prog Mater Sci. 2009;54:397-425.

[4] Liebschner MAK. Biomechanical considerations of animal models used in tissue engineering of bone. Biomaterials. 2004;25:1697-1714.

[5] Niinomi M, Nakai M. Titanium-based biomaterials for preventing stress shielding between implant devices and bone. Int J Biomater. 2011;2011:836587.

[6] Murr LE. Open-cellular metal implant design and fabrication for biomechanical compatibility with bone. J Mech Behav Biomed Mater. 2017;76:164-177.

[7] Wang X, Xu S, Zhou S, Xu W, Leary M, Choong P, et al. Topological design and additive manufacturing of porous metals for bone scaffolds and orthopaedic implants: a review. Biomaterials. 2016;83:127-141.

[8] Ngo TD, Kashani A, Imbalzano G, Nguyen KTQ, Hui D. Additive manufacturing (3D printing): a review of materials, methods, applications and challenges. Compos Part B. 2018;143:172-196.

[9] Karageorgiou V, Kaplan D. Porosity of 3D biomaterial scaffolds and osteogenesis. Biomaterials. 2005;26:5474-5491.

[10] Yuan L, Ding S, Wen C. Additive manufacturing technology for porous metal implant applications and triple minimal surface structures: a review. Bioact Mater. 2019;4:56-70.

[11] iData Research. Global orthopedic devices market report. [Place unknown]: iData Research; 2022.

[12] Vandenbroucke B, Kruth JP. Selective laser melting of biocompatible metals for rapid manufacturing of medical parts. Rapid Prototyp J. 2007;13:196-203.

[13] Tshephe TS, Akinwamide SO, Olevsky E, Olubambi PA. Additive manufacturing of titanium-based alloys: a review of methods, properties, challenges, and prospects. Heliyon. 2022;8:e09041.

[14] Luo B, Miu L, Luo Y. Titanium alloys for biomedical applications: a review on additive manufacturing process and surface modification technology. Int J Adv Manuf Technol. 2025;137:3215-3227.

[15] Kiselevskiy MV, Anisimova NY, Kapustin AV, Ryzhkin AA, Kuznetsova DN, Polyakova VV, et al. Development of bioactive scaffolds for orthopedic applications by designing additively manufactured titanium porous structures: a critical review. Biomimetics. 2023;8:546.

[16] Sidambe AT. Biocompatibility of advanced manufactured titanium implants: a review. Materials. 2014;7:8168-8188.

[17] Li Y, Jiang D, Zhu R, et al. Revolutionizing medical implant fabrication: advances in additive manufacturing of biomedical metals. Int J Extrem Manuf. 2025;7:022002.

[18] Guo C, Ding T, Cheng Y, Zheng J, Fang X, Feng Z. The rational design, biofunctionalization and biological properties of orthopedic porous titanium implants: a review. Front Bioeng Biotechnol. 2025;13:1548675.

[19] Chen H, Han Q, Wang C, Liu Y, Chen B, Wang J. Porous scaffold design for additive manufacturing in orthopedics: a review. Front Bioeng Biotechnol. 2020;8:609.

[20] Distefano F, Pasta S, Epasto G. Titanium lattice structures produced via additive manufacturing for a bone scaffold: a review. J Funct Biomater. 2023;14:125.

[21] Niinomi M. Mechanical properties of biomedical titanium alloys. Mater Sci Eng A. 1998;243:231-236.

[22] Brunette DM, Tengvall P, Textor M, Thomsen P, editors. Titanium in medicine. Berlin: Springer; 2001.

[23] Boyer R, Welsch G, Collings EW, editors. Materials properties handbook: titanium alloys. Materials Park (OH): ASM International; 1994.

[24] Liu X, Chu PK, Ding C. Surface modification of titanium, titanium alloys, and related materials for biomedical applications. Mater Sci Eng R Rep. 2004;47:49-121.

[25] Liu S, Shin YC. Additive manufacturing of Ti6Al4V alloy: a review. Mater Des. 2019;164:107552.

[26] Bauer S, Schmuki P, von der Mark K, Park J. Engineering biocompatible implant surfaces. Part I: materials and surfaces. Prog Mater Sci. 2013;58:261-326.

[27] Niinomi M. Recent metallic materials for biomedical applications. Metall Mater Trans A. 2002;33:477-486.

[28] Hao YL, Li SJ, Sun SY, Zheng CY, Yang R. Elastic deformation behaviour of Ti-24Nb-4Zr-7.9Sn for biomedical applications. Acta Biomater. 2007;3:277-286.

[29] Kuroda D, Niinomi M, Morinaga M, Kato Y, Yashiro T. Design and mechanical properties of new beta type titanium alloys for implant materials. Mater Sci Eng A. 1998;243:244-249.

[30] Zhou L, Yuan T, Li R, Tang J, Wang M, Mei F. Microstructure and mechanical properties of selective laser melted biomaterial Ti-13Nb-13Zr compared to hot-forged Ti-6Al-4V. Mater Sci Eng A. 2018;725:329-340.

[31] DebRoy T, Wei HL, Zuback JS, Mukherjee T, Elmer JW, Milewski JO, et al. Additive manufacturing of metallic components: process, structure and properties. Prog Mater Sci. 2018;92:112-224.

[32] Murr LE, Gaytan SM, Ramirez DA, Martinez E, Hernandez J, Amato KN, et al. Metal fabrication by additive manufacturing using laser and electron beam melting technologies. J Mater Sci Technol. 2012;28:1-14.

[33] Vrancken B, Thijs L, Kruth JP, Van Humbeeck J. Heat treatment of Ti6Al4V produced by selective laser melting: microstructure and mechanical properties. J Alloys Compd. 2012;541:177-185.

[34] Gong H, Rafi K, Gu H, Starr T, Stucker B. Analysis of defect generation in Ti-6Al-4V parts made using powder bed fusion additive manufacturing processes. Addit Manuf. 2014;1-4:87-98.

[35] Gaytan SM, Murr LE, Medina F, Martinez E, Lopez MI, Wicker RB. Advanced metal powder based manufacturing of complex components by electron beam melting. Mater Technol. 2009;24:180-190.

[36] Tan X, Kok Y, Tan YJ, Descoins M, Mangelinck D, Tor SB, et al. Graded microstructure and mechanical properties of additive manufactured Ti-6Al-4V via electron beam melting. Acta Mater. 2015;97:1-16.

[37] Heinl P, Muller L, Korner C, Singer RF, Muller FA. Cellular Ti-6Al-4V structures with interconnected macro porosity for bone implants fabricated by selective electron beam melting. Acta Biomater. 2008;4:1536-1544.

[38] Ding D, Pan Z, Cuiuri D, Li H. Wire-feed additive manufacturing of metal components: technologies, developments and future interests. Int J Adv Manuf Technol. 2015;81:465-481.

[39] du Plessis A, Razavi SMJ, Benedetti M, Murchio S, Leary M, Watson M, et al. Properties and applications of additively manufactured metallic cellular materials: a review. Prog Mater Sci. 2022;125:100918.

[40] Abueidda DW, Bakir M, Abu Al-Rub RK, Bergstrom JS, Sobh NA, Jasiuk I. Mechanical properties of 3D printed polymeric cellular materials with triply periodic minimal surface architectures. Mater Des. 2017;122:255-267.

[41] Gibson LJ, Ashby MF. Cellular solids: structure and properties. 2nd ed. Cambridge: Cambridge University Press; 1997.

[42] Deshpande VS, Ashby MF, Fleck NA. Foam topology: bending versus stretching dominated architectures. Acta Mater. 2001;49:1035-1040.

[43] Ashby MF. The properties of foams and lattices. Philos Trans R Soc A. 2006;364:15-30.

[44] Arabnejad S, Johnston RB, Pura JA, Singh B, Tanzer M, Pasini D. High-strength porous biomaterials for bone replacement: a strategy to assess the interplay between cell morphology, mechanical properties, bone ingrowth and manufacturing constraints. Acta Biomater. 2016;30:345-356.

[45] Yoo DJ. Porous scaffold design using the distance field and triply periodic minimal surface models. Biomaterials. 2011;32:7741-7754.

[46] Yang N, Quan Z, Zhang D, Tian Y. Multi-morphology transition hybridization CAD design of minimal surface porous structures for use in tissue engineering. Comput Aided Des. 2014;56:11-21.

[47] Bobbert FSL, Lietaert K, Eftekhari AA, Pouran B, Ahmadi SM, Weinans H, et al. Additively manufactured metallic porous biomaterials based on minimal surfaces: a unique combination of topological, mechanical, and mass transport properties. Acta Biomater. 2017;53:572-584.

[48] Soro N, Brassart L, Chen Y, Veidt M, Attar H, Dargusch MS. Finite element analysis of porous commercially pure titanium for biomedical implant application. Mater Sci Eng A. 2018;725:43-50.

[49] Zhang XY, Fang G, Leeflang S, Zadpoor AA, Zhou J. Topological design, permeability and mechanical behavior of additively manufactured functionally graded porous metallic biomaterials. Acta Biomater. 2019;84:437-452.

[50] Gibson LJ, Ashby MF. The mechanics of three-dimensional cellular materials. Proc R Soc Lond A. 1982;382:43-59.

[51] Amin Yavari S, Ahmadi SM, Wauthle R, Pouran B, Schrooten J, Weinans H, et al. Relationship between unit cell type and porosity and the fatigue behavior of selective laser melted meta-biomaterials. J Mech Behav Biomed Mater. 2015;43:91-100.

[52] Ahmadi SM, Hedayati R, Li Y, Lietaert K, Tumer N, Fatemi A, et al. Fatigue performance of additively manufactured meta-biomaterials: the effects of topology and material type. Acta Biomater. 2018;65:292-304.

[53] Tancogne-Dejean T, Spierings AB, Mohr D. Additively-manufactured metallic micro-lattice materials for high specific energy absorption under static and dynamic loading. Acta Mater. 2016;116:14-28.

[54] Wauthle R, Vrancken B, Beynaerts B, Jorissen K, Schrooten J, Kruth JP, et al. Effects of build orientation and heat treatment on the microstructure and mechanical properties of selective laser melted Ti6Al4V lattice structures. Addit Manuf. 2015;5:77-84.

[55] Van Hooreweder J, Apers Y, Lietaert K, Kruth JP. Improving the fatigue performance of porous metallic biomaterials produced by selective laser melting. Acta Biomater. 2017;47:193-202.

[56] Pyka G, Burakowski A, Kerckhofs G, Moesen M, Van Bael S, Schrooten J, et al. Surface modification of Ti6Al4V open porous structures produced by additive manufacturing. Adv Eng Mater. 2012;14:363-370.

[57] Petite H, Viateau V, Bensaid W, Meunier A, de Pollak C, Bourguignon M, et al. Tissue-engineered bone regeneration. Nat Biotechnol. 2000;18:959-963.

[58] Hutmacher DW. Scaffolds in tissue engineering bone and cartilage. Biomaterials. 2000;21:2529-2543.

[59] Hollister SJ. Porous scaffold design for tissue engineering. Nat Mater. 2005;4:518-524.

[60] Bose S, Roy M, Bandyopadhyay A. Recent advances in bone tissue engineering scaffolds. Trends Biotechnol. 2012;30:546-554.

[61] Kapat K, Srivas PK, Rameshbabu AP, Maity P, Jana S, Dutta J, et al. Influence of porosity and pore-size distribution in Ti6Al4V foam on physicomechanical properties, osteogenesis,

and quantitative validation of bone ingrowth by micro-computed tomography. ACS Appl Mater Interfaces. 2017;9:39235-39248.

[62] Ran Q, Yang W, Hu Y, Shen X, Yu Y, Xiang Y, et al. Osteogenesis of 3D printed porous Ti6Al4V implants with different pore sizes. J Mech Behav Biomed Mater. 2018;84:1-11.

[63] Luan HJ, Wang XM, Zhang K, Li MW, Liu XY, Liu YS, et al. Bone behavior on micron-pore titanium implants by selective laser melting: an in vivo experiment. Med Sci Monit. 2020;26:e924011.

[64] Ryan GE, Pandit AS, Apatsidis DP. Porous titanium scaffolds fabricated using a rapid prototyping and powder metallurgy technique. Biomaterials. 2008;29:3625-3635.

[65] Mour M, Das D, Winkler T, Hoenig E, Mielke G, Morlock MM, et al. Advances in porous biomaterials for dental and orthopaedic applications. Materials. 2010;3:2947-2974.

[66] Van Bael S, Chai YC, Truscello S, Moesen M, Kerckhofs G, Van Oosterwyck H, et al. The effect of pore geometry on the in vitro biological behavior of human periosteum-derived cells seeded on selective laser-melted Ti6Al4V bone scaffolds. Acta Biomater. 2012;8:2824-2834.

[67] Deligianni DD, Katsala N, Ladas S, Sotiropoulou D, Amedee J, Missirlis YF. Effect of surface roughness of the titanium alloy Ti-6Al-4V on human bone marrow cell response and on protein adsorption. Biomaterials. 2001;22:1241-1251.

[68] Mani G, Feldman MD, Patel D, Agrawal CM. Coronary stents: a materials perspective. Biomaterials. 2007;28:1689-1710.

[69] Truscello AS, Kerckhofs G, Van Bael S, Pyka G, Schrooten J, Van Oosterwyck H. Prediction of permeability of regular scaffolds for skeletal tissue engineering: a combined computational and experimental study. Acta Biomater. 2012;8:1648-1658.

[70] Le Guehennec L, Soueidan A, Layrolle P, Amouriq Y. Surface treatments of titanium dental implants for rapid osseointegration. Dent Mater. 2007;23:844-854.

[71] Khudhair D, Bhatti A, Li Y, Hamedani HA, Garmestani H, Hodgson P, et al. Anodization parameters influencing the morphology and electrical properties of TiO2 nanotubes for living cell interfacing and investigations. Mater Sci Eng C. 2016;59:1125-1142.

[72] Park J, Bauer S, von der Mark K, Schmuki P. Nanosize and vitality: TiO2 nanotube diameter directs cell fate. Nano Lett. 2007;7:1686-1691.

[73] Bose S, Tarafder S. Calcium phosphate ceramic systems in growth factor and drug delivery for bone tissue engineering: a review. Acta Biomater. 2012;8:1401-1421.

[74] Surmenev RA, Surmeneva MA, Ivanova AA. Significance of calcium phosphate coatings for the enhancement of new bone osteogenesis: a review. Acta Biomater. 2014;10:557-579.

[75] Yang Y, Hulbert MF, Norris AD, Johnson P, Smith T. Local drug delivery from porous titanium implants for orthopedic applications: a review. Mater Sci Eng C. 2021;122:111900. [Metadata not verified; replace if the source cannot be located.]

[76] Stadelmann VA, Terrier A, Pioletti DP. Microstimulation at the bone-implant interface upregulates osteoclast activation pathways. Bone. 2008;42:358-364.

[77] Slotwinski J, Garboczi E, Stutzman P, Ferraris C, Watson S, Peltz M. Characterization of metal powders used for additive manufacturing. J Res Natl Inst Stand Technol. 2014;119:460-493.

[78] King WE, Anderson AT, Ferencz RM, Hodge NE, Kamath C, Khairallah SA, et al. Laser powder bed fusion additive manufacturing of metals: physics, computational, and materials challenges. Appl Phys Rev. 2015;2:041304.

[79] Tang M, Pistorius PC, Beuth JL. Prediction of lack-of-fusion porosity for powder bed fusion. Addit Manuf. 2017;14:39-48.

[80] Pyka G, Kerckhofs G, Papantoniou I, Speirs M, Schrooten J, Wevers M. Surface roughness and morphology customization of additive manufactured open porous Ti6Al4V structures. Materials. 2013;6:4737-4757.

[81] du Plessis A, Macdonald E. Hot isostatic pressing in metal additive manufacturing: X-ray tomography reveals details of pore closure. Addit Manuf. 2020;34:101191.

[82] Everton SK, Hirsch M, Stravroulakis P, Leach RK, Clare AT. Review of in-situ process monitoring and in-situ metrology for metal additive manufacturing. Mater Des. 2016;95:431-445.

[83] Scime L, Beuth J. A multi-scale convolutional neural network for autonomous anomaly detection and classification in a laser powder

bed fusion additive manufacturing process. Addit Manuf. 2018;24:273-286.

[84] Sing N, Singh S, Ramakrishna S. Biomedical applications of additive manufacturing: present and future. Curr Opin Biomed Eng. 2017;2:105-115.

[85] Provaggi M, Leong JJC, Kalaskar DM. Applications of 3D printing in the management of severe spinal conditions. Proc Inst Mech Eng H. 2017;231:471-486.

[86] Castagnini F, Bordini B, Stea C, Calderoni A, Masetti A, Traina F. Highly porous titanium cup in cementless total hip arthroplasty: registry results at eight years. Int Orthop. 2019;43:1815-1821.

[87] Wang L, Cao X, Han X, et al. Patient-specific 3D-printed prostheses for limb salvage and reconstruction after bone tumor resection. J Bone Oncol. 2022;33:100431.

[88] Parthasarathy J. 3D modeling, custom implants and its future perspectives in craniofacial surgery. Ann Maxillofac Surg. 2014;4:9-18.

[89] Tunchel S, Blay A, Kolerman R, Mijiritsky E, Shibli JA. 3D-printing of titanium dental implants: current and future trends. Int J Dent. 2016;2016:8590971.

[90] US Food and Drug Administration. Technical considerations for additive manufactured medical devices: guidance for industry and Food and Drug Administration staff. Silver Spring (MD): FDA; 2017.

[91] Di Prima M, Coburn J, Hwang D, Kelly J, Khairuzzaman A, Ricles L. Additively manufactured medical products: the FDA perspective. 3D Print Med. 2016;2:1.

[92] Zheng YF, Gu XN, Witte F. Biodegradable metals. Mater Sci Eng R Rep. 2014;77:1-34.

[93] Robinson DA, Griffith RW, Shechtman D, Evans RB, Conzemius MG. In vitro antibacterial properties of magnesium metal against Escherichia coli, Pseudomonas aeruginosa and Staphylococcus aureus. Acta Biomater. 2010;6:1869-1877.

[94] Chen H, Liu Y, Wang C, Zhang Y, Chen B, Wang J. Design and properties of biomimetic irregular scaffolds for bone tissue engineering based on Voronoi-tessellation. Mater Des. 2022;218:110670.

[95] Zhang X, Tang B, Wei B, Li Y, Lei S, Liu X, et al. Topology optimization driven by deep learning for accelerated additive-manufactured scaffold design. Comput Methods Appl Mech Eng. 2023;412:116091. [Metadata not verified; check before submission.]

[96] Bandyopadhyay A, Espana F, Balla VK, Bose S, Ohgami Y, Davies NM. Influence of porosity on mechanical properties and in vivo response of Ti6Al4V implants. Acta Biomater. 2010;6:1640-1648.

[97] Zadpoor AA. Mechanical performance of additively manufactured meta-biomaterials. Acta Biomater. 2019;85:41-59.

[98] Knapp GL, Mukherjee T, Zuback JS, Wei HL, Palmer TA, De A, et al. Building blocks for a digital twin of additive manufacturing. Acta Mater. 2017;135:390-399.

[99] Barba D, Alabort E, Reed RC. Synthetic bone: design by additive manufacturing. Acta Biomater. 2019;97:637-656.

[100] Benedetti M, du Plessis A, Ritchie RO, Dallago M, Razavi N, Berto F. Architected cellular materials: a review on their mechanical properties towards fatigue-tolerant design and fabrication. Mater Sci Eng R Rep. 2021;144:100606.

[101] Geng Z, Cui Z, Li Z, Zhu S, Liang Y, Liu Y, et al. Strontium incorporation to optimize the antibacterial and biological characteristics of silver-substituted hydroxyapatite coating. Mater Sci Eng C Mater Biol Appl. 2016;58:467-477.

[102] Pal S, Lojen G, Hudak R, Rajtukova V, Brajlih T, Kokol V, et al. As-fabricated surface morphologies of Ti-6Al-4V samples fabricated by different laser processing parameters in selective laser melting. Addit Manuf. 2020;33:101147.

[103] Geng X, Li Y, Li F, Wang X, Zhang K, Liu Z, et al. A new 3D printing porous trabecular titanium metal acetabular cup for primary total hip arthroplasty: a minimum 2-year follow-up of 92 consecutive patients. J Orthop Surg Res. 2020;15:383